

## Numerical Analysis of Light Extraction Efficiency of a Core-shell Nanorod Light-emitting Diode

Kangseok Kim<sup>†</sup>, Gijun Ju<sup>†</sup>, and Younghyun Kim\*

*Department of Photonics and Nanoelectronics, Hanyang University, Ansan 15588, Korea*

(Received April 24, 2023 : revised June 21, 2023 : accepted July 14, 2023)

We present a detailed analysis of the light extraction efficiency (LEE) of a core-shell nanorod light emitting diode (LED) using finite-difference time-domain (FDTD) simulations. We found that the LEE has a deep dependence on source positions and polarization directions based on the calculated LEE results for every  $x$  and  $z$  position inside the core-shell nanorod structure. The LEEs are different for the upper part (pyramid) and the lower part (sidewall) of the core-shell nanorod owing to total internal reflection (TIR) and the generated optical modes in the structure. As a result, the LEE of sidewall is much larger than that of pyramid. The averaged LEE of the core-shell nanorod LED is also investigated with variable  $p$ -GaN thickness,  $n$ -GaN thickness, and height for the design guidelines for the optimized LEE of core-shell nanorod LEDs.

**Keywords :** Core-shell nanorod LED, FDTD analysis, Light extraction efficiency

**OCIS codes :** (050.1755) Computational electromagnetic methods; (230.0230) Optical devices; (230.3670) Light-emitting diodes

### I. INTRODUCTION

With the advancement in display technology, inorganic micro-light emitting diodes (LEDs) have attracted great attention as a promising display light source because they promise lower power consumption, a longer life span, and faster response time compared to organic LEDs [1–3]. Recently, there have been many studies to reduce the size of micro-LEDs even more with the growing requirement for high resolution in next-generation displays such as virtual reality (VR) and augmented reality (AR) applications [4, 5]. the technology roadmap is continuing to nano-size LEDs not only because of further demands in display technology but also for the increase in device integration density [6, 7]. In addition, the potential of nano-scale LEDs for more efficient electrical and optical performance of novel device architectures, such as nano-ring LEDs, nano-needle LEDs, and even nanorod LEDs has been growing compared to

conventional LEDs [8–10].

Gallium nitride (GaN)-based LEDs, which have wide coverage of light-emitting colors using bandgap manipulation, have progressed remarkably over the last two decades since the first application of LEDs in the early 1990s [11, 12]. However, in conventional GaN-based LEDs, performance is still restricted owing to the threading dislocation caused by the lattice mismatch between the GaN and the substrate, and the quantum-confined Stark effect (QCSE) in multiple quantum wells (MQW) [13–15]. This QCSE leads to a spatial separation of the electron and hole wave functions and a decline in the transition energy between them [15–18]. Regarding that, a core-shell nanorod structure, which was demonstrated in the references [19, 20], is considered a very promising solution to avoid the degradation caused by the QCSE and threading dislocation, resulting in high efficiency [21]. While the conventional planar LED has been grown on a  $c$ -plane, the GaN-based core-shell

<sup>†</sup>These authors contributed equally to this paper.

\*Corresponding author: younghyunkim@hanyang.ac.kr, ORCID 0000-0001-8072-1251

Color versions of one or more of the figures in this paper are available online.



This is an Open Access article distributed under the terms of the Creative Commons Attribution Non-Commercial License (<http://creativecommons.org/licenses/by-nc/4.0/>) which permits unrestricted non-commercial use, distribution, and reproduction in any medium, provided the original work is properly cited.

Copyright © 2023 Current Optics and Photonics

nanorod LED can be grown on a non-polar or semi-polar plane, leading it to be free from the internal polarization field [20, 21]. Furthermore, an improvement of optical properties is also expected because the core-shell nanorod structure has an enlarged active area and reduced dislocation density due to a high aspect ratio and reduced influences of thermal and lattice mismatch, respectively [22–26].

Since the performance of conventional LEDs has been improved by maximizing the external quantum efficiency (EQE), it should also be developed for highly efficient nano LEDs. The external quantum efficiency (EQE) is described below:

$$\eta_{\text{EQE}} = \eta_{\text{IQE}} \times \eta_{\text{LEE}}, \quad (1)$$

where  $\eta_{\text{EQE}}$  is how many photons emit to free space compared to total electrons injected into the LED. In Eq. (1), the EQE is the product of internal quantum efficiency (IQE) and light extraction efficiency (LEE). LEE is defined as the proportion of the number of photons emitted to free space from the LED to the number of photons emitted from the active region inside the LED [27]. As can be seen in Eq. (1), LEE is considered one of the most important parameters to achieve high EQE. Since LEE strongly depends on its structure, it is important to understand how the generated light or photons escape from the nanostructure so that it can be designed for high LEE.

The current white LEDs face several limitations due to the use of yellow phosphors, which result in color conversion loss, low color rendering index, and increased costs. The GaN-based core-shell nanorod white LED has emerged as a promising alternative to overcome these limitations [28, 29], because it has a broad photoluminescence intensity due to the involvement of the pyramid top of the core-shell nanorod in longer wavelengths [29]. However, the lack of quantitative understanding of light extraction in the core-shell nanostructures is a growing concern that needs to be addressed. Our study aims to narrow this knowledge gap and contribute to the development of highly efficient next-generation display technology with tens of millions of nano LEDs, making it a timely and significant research endeavor.

## II. SIMULATION METHOD

For the simulations in this study, we employed a commercially available finite-difference time-domain (FDTD) simulation solver (Lumerical Inc., BC, Canada), known for its reliability in the numerical analysis of photonic components. To ensure accurate simulation results for the core-shell nanorods, we meticulously considered specific parameters such as the optical constants of GaN and InGaN in the emission wavelength range (details are given later) as well as mesh accuracy and convergence for the 3D FDTD simulation conditions [30]. Three-dimensional illustrations of the GaN-based core-shell nanorod LED and its interior are shown in Fig. 1(a). The dipole source positions are also marked in the figure. At each position, a dipole source is considered in three directions of the  $x$ -,  $y$ -, and  $z$ -axis for the accurate simulation of the nanorod LED in which the translational symmetry is no longer maintained [31]. Since the surfaces of the hexagonally structured nanorod are symmetric and the surface is also bisymmetric, the LEE regarding half of one surface was simulated as shown in Fig. 1(a). We named the top of the core-shell nanorod structure pyramid and the bottom of it sidewall. FDTD simulations at each position on sidewall and pyramid were conducted by varying the dipole source positions along with the  $x$ - and  $z$ -direction. On the other hand, the  $y$ -direction is neglected because of the very thin MQW layer thickness, typically a few tens of nanometers [32]. Figure 1(b) shows a schematic side view of the core-shell nanorod structure and computational domain. The simulated core-shell nanorod LED structure is exposed to air and applied to the perfectly matched layers (PMLs) in all boundaries of the FDTD simulation domain so that propagating light is entirely absorbed in the PML. The Poynting vectors used in the LEE calculation are analyzed on the detection plane in PML as seen in Fig. 1(b).

The GaN-based core-shell nanorod LED grown on the  $n$ -GaN substrate consists of a  $n$ -GaN main rod ( $R_1 = 145$  nm), an InGaN/GaN MQW shell ( $R_2 = 175$  nm), and a  $p$ -GaN shell ( $R_3 = 225$  nm) outside of the rod, and the fixed height ( $h = 4.6 \mu\text{m}$ ) as depicted in Fig. 1(c). The structure parameters

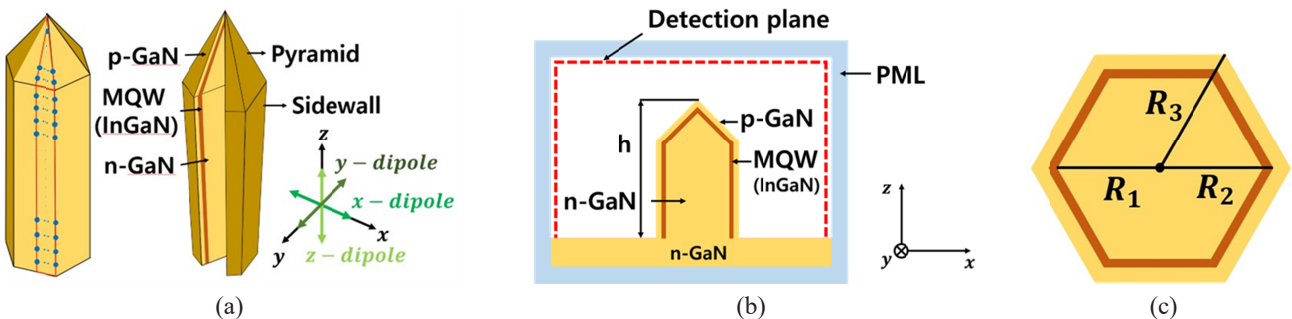


**FIG. 1.** Structure maps in the FDTD simulation. (a) 3D schematic of core-shell nanorod for internal configuration and dipole source positions marked on the surfaces, (b) side view, and (c) cross-section of GaN-based core-shell nanorod structure. FDTD simulation range enclosed by PML. FDTD, finite-difference time-domain; PML, perfectly matched layer.

were chosen considering the experimental demonstration [23]. The wavelengths emitted from a dipole source were set at 440 nm to 460 nm in sidewall and at 495 nm to 515 nm in pyramid [33]. The spectrum intensity of a dipole source is a Gaussian shape with each peak intensity at 450 nm, and 505 nm in the sidewall and pyramid, respectively. Since the emission wavelengths differ depending on the In mole fraction in the MQW, it was set depending on the region. The effective refractive index of GaN is 2.48 and 2.42 as the emission wavelength ranges from 440 nm to 460 nm and from 495 nm to 515 nm, respectively [34]. The In mole fraction in the MQW shell is 10% in sidewall and 20% in pyramid [35]. The refractive index of InGaN/GaN active regions in sidewall is 2.54 and 2.45 for the wavelength ranges of 440 nm to 460 nm and 495 nm to 515 nm, respectively [36]. In pyramid, the refractive index of the MQW is 2.62 and 2.68 for the same wavelength range [36]. In general, dispersion was taken into account based on wavelength and position. Since the GaN layer has a wide bandgap and cannot absorb light at the setting wavelength, the extinction coefficient of GaN was set to zero [37]. Another extinction coefficient of the InGaN MQW layer was calculated for each wavelength using the following equation [38]:

$$k_e = \frac{\lambda}{4\pi} \alpha. \quad (2)$$

Here,  $k_e$  is defined as the extinction coefficient.  $\lambda$  and

$\alpha$  are also defined as the wavelength and absorption coefficient, respectively. The absorption coefficient of InGaN was based on the reference data [36].

The LEE at position  $(x, y, z)$  with each polarization in the MQW is calculated by the

$$T(f) = \frac{\frac{1}{2} \int_{\text{monitor}} \text{Re}(\mathbf{P}(f)) \cdot dS}{\text{sourcepower}(f)}, \quad (3)$$

where  $T(f)$  is the normalized transmission as a function of frequency and  $\mathbf{P}$  is the Poynting vector, meaning that the amount of power transmitted through power monitors and profile monitors normalized to the source power is obtained.

### III. RESULTS AND DISCUSSION

Figures 2(a) and 2(b) show the simulation results of LEE as a function of  $x$ -position for sidewall and pyramid, respectively. Three sources of  $x$ -,  $y$ -, and  $z$ -polarization of LEE are plotted as a function of the  $x$ -position from the left-hand to right-hand sides. For sidewall in Fig. 2(a), the LEE of  $x$ -polarization decreases slightly with an increasing  $x$ -position but is almost constant at around 30%. The LEEs of  $y$ - and  $z$ -polarization vary from 35% to 50% and from 20% to 35%, respectively. We did not include the light directed toward the substrate in the detection plane because

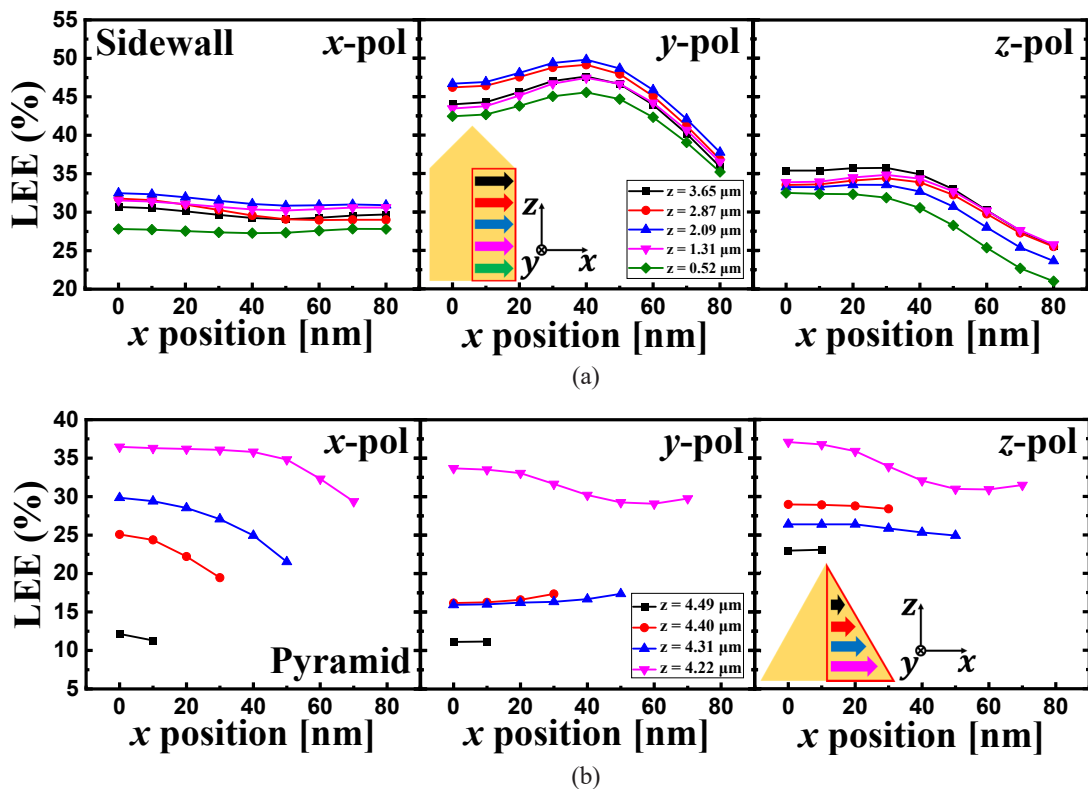


**FIG. 2.** Light extraction efficiency (LEE) vs. source position in the (a) sidewall or (b) pyramid for the  $x$ -position with dipole sources polarized in the  $x$ -,  $y$ -, and  $z$ -directions.

we focused on how effectively the light emitted from the MQW layer escapes into the air. However, the maximum LEE would be larger if the light toward the substrate was designed to be reflected [39]. The three polarizations show similar dependency in which the LEE decreases with an increase in the  $x$ -position. For pyramid in Fig. 2(b), the LEEs show a similar trend of decrease with an increase in  $x$ -position, but they show larger  $z$ -position dependency due to its geometrical effect compared to those of sidewall.

The LEE depending on the dipole polarization and source position is closely related to the resonant optical modes inside the core-shell nanorod, which affect the optical properties in the cavity. Regarding that, whispering gallery mode (WGM) is one of the resonant modes in the nano-rod cavity structure arising from the interference with light circulating inside the curvature of the structure boundaries by total internal reflection (TIR) [40, 41]. WGM is usually generated in a circular structure or dome, but it is also formed even in hexagonal structures [41]. The position and size of WGMs depend on the shape and size of the core structure. When a dipole source is positioned where the electric field is strongest due to the WGM's optical confinement, the emitted light travels along with the circumstance of the structure and escapes from it very slowly [40, 41].

Figure 3 shows the electric field intensity profile of the  $x$ - $y$  plane. The top and bottom profiles are when the dipole is located at  $x = 0$  nm and  $x = 80$  nm, respectively. To provide a more comprehensive comparison, the mode profiles are displayed in relative intensity using a reduced scale, so that the optical modes on the circumference clearly appear within a limited intensity scale. Figure 3(a) presents the electric field intensity profile of the  $x$ - $y$  plane when the dipole is on sidewall and oscillates in the  $z$ -direction. The light is more confined in the structure circularly due to the property of the WGM as mentioned earlier. In addition,

similar results were observed for the  $y$ -polarization. Thus, it will be the root of the decrease of LEE in the cases of  $y$ - and  $z$ -polarization in Fig. 2(a). However, as mentioned above, the decrease in LEE for  $y$ - and  $z$ -polarization is not substantial due to the significant reduction in intensity scale, unlike the displayed mode profiles.

Figure 3(b) is a similar condition to Fig. 3(a), but the dipole is placed in pyramid. The result shows that the emitted light is more confined along with the increasing  $x$ -position. Hence, LEE is reduced, as shown in Fig. 2(b). The difference in the WGM between sidewall and pyramid is that sidewall shows a clear mode, while pyramid shows a blurred mode, meaning that the WGM is formed stronger in sidewall than in pyramid. Therefore, the decrease in LEE for sidewall is larger than that for pyramid. Figure 3(c) shows the electric field intensity profile of  $x$ -polarization. Unlike,  $y$ - and  $z$ -polarization, the WGM is not observed regardless of the dipole position on the  $x$ -axis. It will be a reason for the almost constant LEE with variable  $x$ -positions, as mentioned in Fig. 2(a).

Figures 4(a) and 4(b) show the LEE results as a function of the  $z$ -position for sidewall and pyramid, respectively. The three figures are for  $x$ -,  $y$ -, and  $z$ -polarization in order from left to right. In Fig. 4(a), the LEEs of the three polarizations fluctuate along with the  $z$ -direction. They are roughly 30%, 45%, and 30% for  $x$ -,  $y$ -, and  $z$ -polarization, respectively. Furthermore, the fluctuation variation between a maximum and minimum value is approximately 2.5%. The LEE of  $y$ -polarization is higher than that of  $x$ - and  $z$ -polarization, like the results in Fig. 2(a). In Fig. 4(b), the results are simulated with the same conditions as shown in Fig. 4(a), but the dipole source is located at the center of the MQW in pyramid. The LEEs for all polarizations significantly decrease with an increasing  $z$ -position.

The refractive index of GaN is much larger than that of

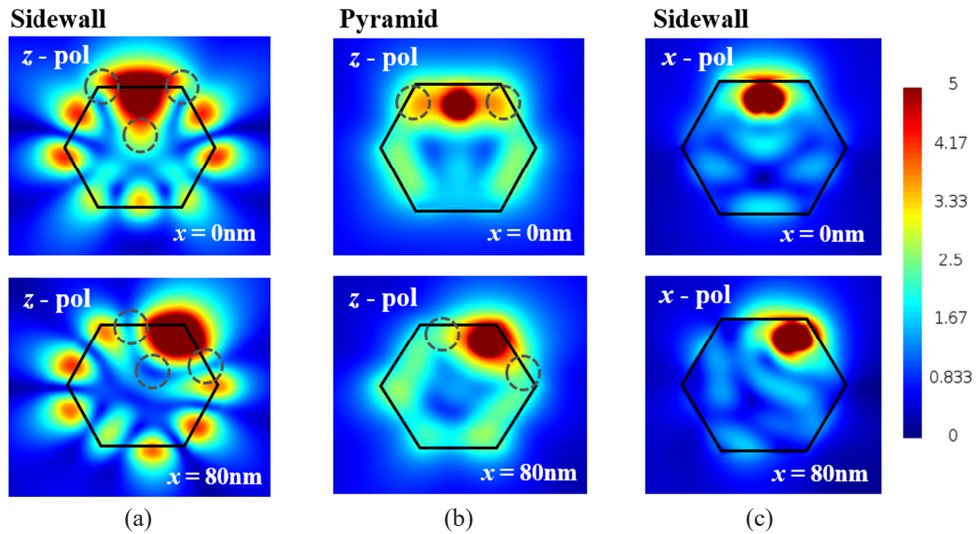


**FIG. 3.** Electric field distributions viewed from the top. (a), (b) Electric field intensity distribution when  $z$ -polarization is in sidewall and pyramid respectively. (c) Electric field intensity distribution when  $x$ -polarization is in sidewall. The upper and lower profile indicate when the dipole source is located at  $x = 0$  nm and  $x = 80$  nm, respectively.

air, so multi modes can be induced in a core-shell nanorod structure like a waveguide. These multi modes lead to the formation of a specific propagating mode owing to the difference in inherent speed. When light is coupled with the propagating mode, it can be relatively easy to escape the core-shell nanorod structure. In other words, a high or low LEE appears when the dipole source position matches the high or low magnitude of the mode [31]. In Fig. 5(a), the electric field distribution viewed from the center of the  $x$ -axis shows the vertical propagation mode when the dipole is placed on sidewall. The vertical propagation mode formed a periodical array with intense domains, resulting

in the fluctuation of LEE for the  $z$ -direction, as mentioned above.

To investigate the significant decrease in LEE depending on the  $z$ -position for pyramid in Fig. 4(b), the electric field intensity profiles of the  $x$ - $z$  plane were analyzed with the two dipole source positions of  $z = 4.22 \mu\text{m}$  and  $4.49 \mu\text{m}$ , near the bottom and top of pyramid, respectively, in Fig. 5(b). It reveals that the light can escape the structure through pyramid and the top of sidewall in the left-hand distribution, while the light is confined inside the nanorod except in adjacent regions of the peak of pyramid in the right-hand distribution. This result would be also explained

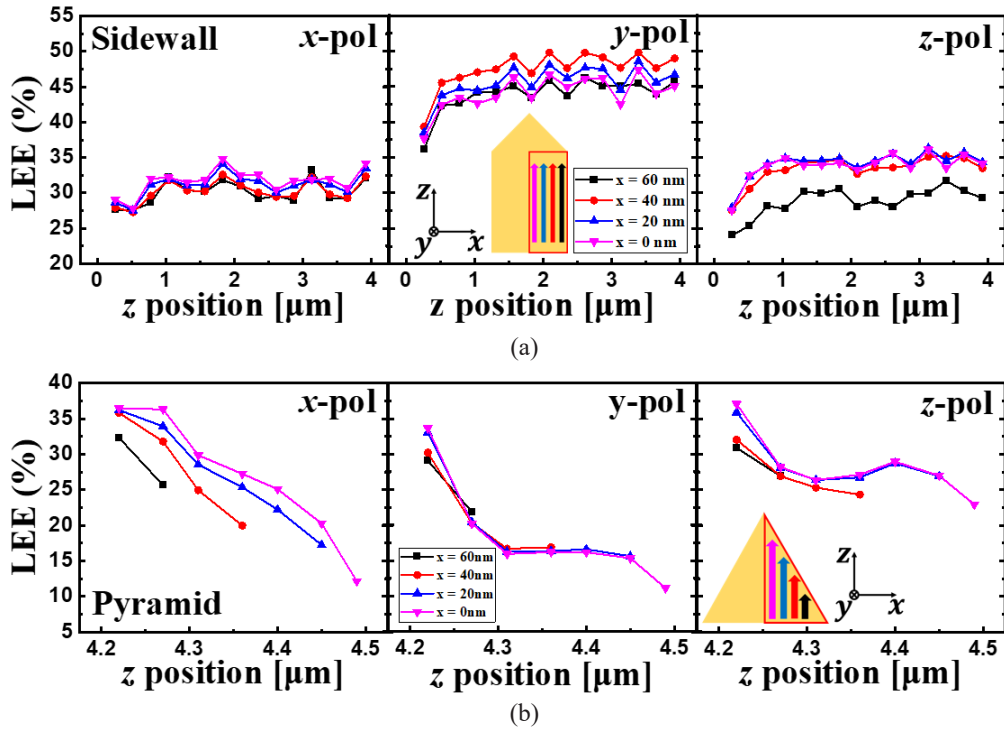


**FIG. 4.** Light extraction efficiency (LEE) vs. source position in (a) sidewall or (b) pyramid for the  $z$ -position with dipole sources polarized in the  $x$ -,  $y$ -, and  $z$ -direction.

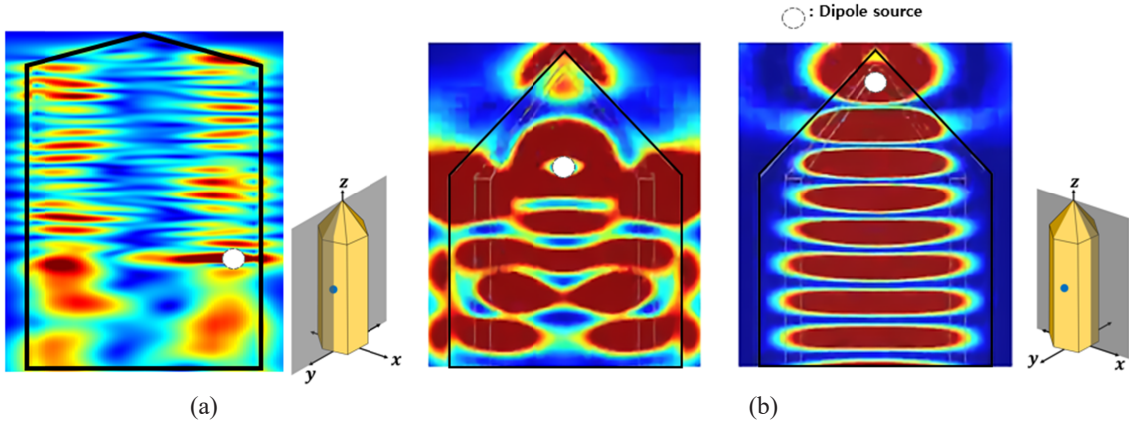


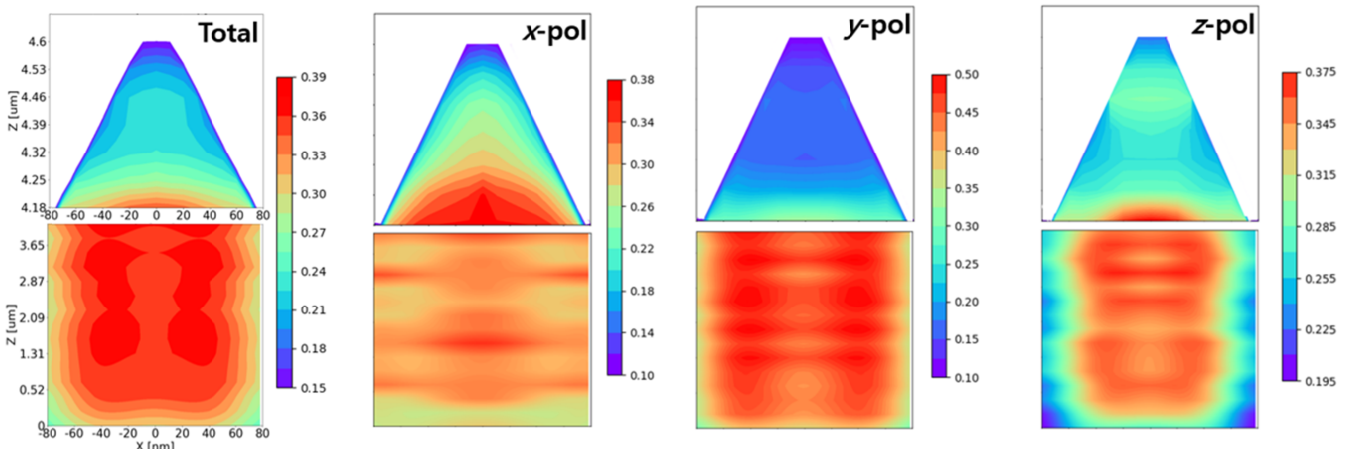
**FIG. 5.** Electric field distributions viewed from the side. (a) Electric field intensity distribution of the  $y$ - $z$  plane; (b) Electric field intensity distribution of the  $x$ - $z$  plane with the dipole sources on the bottom ( $z = 4.22 \mu\text{m}$ ) and top ( $z = 4.49 \mu\text{m}$ ) of pyramid.

by the TIR as the dipole source's  $z$ -position increased. Using the formula of the TIR,  $\theta_c = \sin^{-1}(n_i/n_i)$ , the angle is obtained to 24.4 degrees. The refraction indices of GaN and air were set at 2.42 and 1. The thickness of InGaN is too thin and the indices difference is too low to be considered. Considering the calculated angle of TIR, the emitted light in the top region is reflected more than in the bottom region as the  $z$ -position of the dipole source goes up. The results are identical to the profile analysis in Fig. 5(b), thus resulting in the decline of LEE in accordance with the height of pyramid. Furthermore, the higher LEE of the  $y$ -polarization dipole is attributed to the difference in oscillation direction. Unlike the other two dipoles, the vibration direction of the  $y$ -polarized dipole is perpendicular to the plane. This distinction leads to the power being radiated parallel to the plane, while the power from  $x$ - and  $z$ -polarization is directed into the structure orthogonally to the oscillation direction. Due to the formation of optical modes within the structure, the  $x$ - and  $z$ -polarized dipole encounters limitations in terms of light extraction. Therefore, the  $y$ -polarized dipole is less affected by the optical modes that existed in-

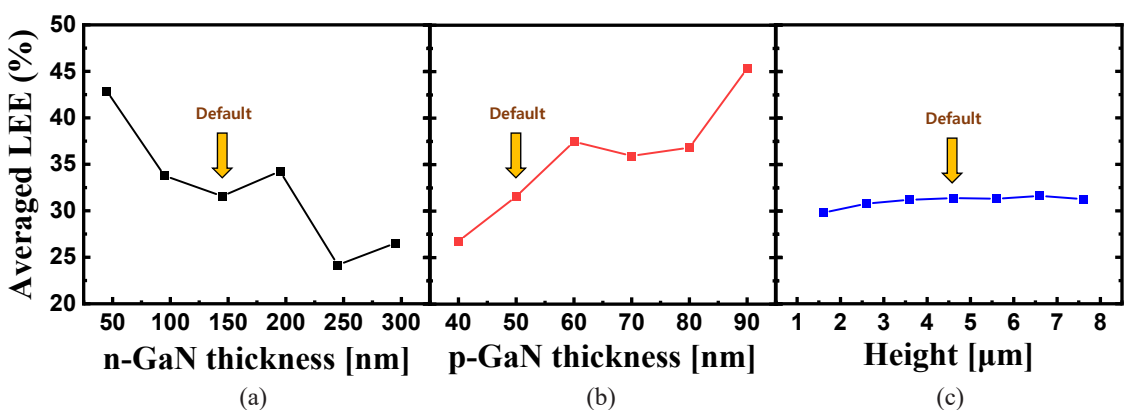
side the structure, resulting in a higher LEE.

Figure 6 shows the LEE distribution in pyramid and sidewall for  $x$ -,  $y$ -,  $z$ -polarization, and their total. As mentioned earlier, sidewall shows larger LEE values compared to pyramid for all polarizations. In addition, the  $y$ -polarized light shows the highest LEE for sidewall, but the lowest for pyramid. It suggests that sidewall and  $y$ -polarization are important design considerations for highly efficient core-shell nanorod LEDs.

We also explored the averaged LEE considering the important parameters of  $n$ -GaN thickness,  $p$ -GaN thickness, and height for design optimization guidelines. LEE was averaged from the whole positions and polarization. Figure 7 shows the averaged LEE as a function of  $n$ -GaN thickness,  $p$ -GaN thickness, and height. The averaged LEE has the opposite tendency for the  $n$ -GaN thickness in Fig. 7(a) and  $p$ -GaN thickness in Fig. 7(b). Their tendency could be attributed to the shift in the relative MQW position. As the  $n$ -GaN thickness decreases, the light can easily escape due to the weak WGM. Similarly, as the  $p$ -GaN thickness increases, the longer distance between the dipole source and



**FIG. 6.** From left, light extraction efficiency (LEE) dimensional distribution of the whole,  $x$ -polarization,  $y$ -polarization, and  $z$ -polarization.



**FIG. 7.** The averaged light extraction efficiency (LEE) is plotted as a function of (a)  $n$ -GaN thickness, (b)  $p$ -GaN thickness, and (c) height for optimization. The fundamental structure of our study is expressed as default.

the air shrinks the WGM so that more light can escape the core-shell nanorod structure. Although height is an important parameter determining active area, there is no significant change in the averaged LEE, as shown in Fig. 7(c). It will be the same reason as discussed in Fig. 4(a) because the height is along the  $z$ -direction.

As a result, we suggest the optimum core-shell nanorod LED with thin  $n$ -GaN thickness and thick  $p$ -GaN thickness so that the MQW is positioned as far from the surface as possible due to the relationship between the averaged LEE and the WGM. Also, when one designs the height of the core-shell nanorod LED, the active light-emitting area will only be needed to consider assuming a constant LEE.

#### IV. CONCLUSION

In this study, we investigated LEE in a GaN-based core-shell nanorod LED structure using the FDTD simulation. It was revealed that LEE has a strong dependence on source positions and polarization directions based on the calculated LEE results for every  $x$ - and  $z$ -position inside the core-shell nanorod structure. For pyramid and sidewall of the core-shell nanorod, the LEEs are different owing to TIR and the generated optical modes in the structure. Consequently, the LEE of sidewall is much larger than that of pyramid. The averaged LEE of the core-shell nanorod LED was also investigated with variable  $p$ -GaN thickness,  $n$ -GaN thickness, and height for the design guidelines for the optimized LEE of core-shell nanorod LEDs.

#### FUNDING

Korea Basic Science Institute (National Research Facilities and Equipment Center) grant funded by the Ministry of Education (grant No. 2023R1A6C103A035, No. 2021R1A-6C101A405); Technology Innovation Program (20015909) through the Korea Evaluation Institute of Industrial Technology (KEIT), funded by the Ministry of Trade, Industry & Energy (MOTIE, Korea); National Research Foundation of Korea (NRF) funded by the Korea government (MSIT) (No. 2021R1G1A1091912, No. 2022K1A3A1A79090726); Korea Institute for Advancement of Technology (KIAT) grant funded by the Korea Government (MOTIE) (P0023718, HRD Program for Industrial Innovation).

#### DISCLOSURES

The authors declare no conflict of interest.

#### DATA AVAILABILITY

Data underlying the results presented in this paper are not publicly available at the time of publication but may be obtained from the authors upon reasonable request.

#### REFERENCES

- Z. Chen, S. Yan, and C. Danesh, "MicroLED technologies and applications: Characteristics, fabrication, progress, and challenges," *J. Phys. D: Appl. Phys.* **54**, 123001 (2021).
- Z. Liu, C.-H. Lin, B.-R. Hyun, C.-W. Sher, Z. Lv, B. Luo, F. Jiang, T. Wu, C.-H. Ho, H.-C. Kuo, and J.-H. He, "Micro-light-emitting diodes with quantum dots in display technology," *Light: Sci. Appl.* **9**, 83 (2020).
- A. R. Anwar, M. T. Sajjad, M. A. Johar, C. A. Hernández-Gutiérrez, M. Usman, and S. P. Lepkowski, "Recent progress in micro-LED-based display technologies," *Laser Photonics Rev.* **16**, 210047 (2022).
- Z. Gong, S. Jin, Y. Chen, J. McKendry, D. Massoubre, I. M. Watson, E. Gu, and M. D. Dawson, "Size-dependent light output, spectral shift, and self-heating of 400 nm InGaN light-emitting diodes," *J. Appl. Phys.* **107**, 013103 (2010).
- J. Xiong, E.-L. Hsiang, Z. He, T. Zhan, and S.-T. Wu, "Augmented reality and virtual reality displays: emerging technologies and future perspectives," *Light: Sci. Appl.* **10**, 216 (2021).
- H. Perlman, T. Eisenfeld, and A. Karsenty, "Performance enhancement and applications review of nano light emitting device (LED)," *Nanomaterials* **11**, 23 (2020).
- A. Waag, X. Wang, S. Fündling, J. Ledig, M. Erenburg, R. Neumann, M. Al Suleiman, S. Merzsch, J. Wei, S. Li, H. H. Wehmann, W. Bergbauer, M. Straßburg, A. Trampert, U. Jahn, and H. Riechert, "The nanorod approach: GaN NanoLEDs for solid state lighting," *Phys. Status Solidi C* **8**, 2296–2301 (2011).
- J. Bai, Q. Wang, and T. Wang, "Greatly enhanced performance of InGaN/GaN nanorod light emitting diodes," *Phys. Status Solidi A* **209**, 477–480 (2012).
- S.-W. Wang, K.-B. Hong, Y.-L. Tsai, C.-H. Teng, A.-J. Tzou, Y.-C. Chu, P.-T. Lee, P.-C. Ku, C.-C. Lin, and H.-C. Kuo, "Wavelength tunable InGaN/GaN nano-ring LEDs via nanosphere lithography," *Sci. Rep.* **7**, 42962 (2017).
- L. C. Chuang, F. G. Sedgwick, R. Chen, W. S. Ko, M. Moewe, K. W. Ng, T. T. D. Tran, and C. Chang-Hasnain, "GaAs-based nanoneedle light emitting diode and avalanche photodiode monolithically integrated on a silicon substrate," *Nano Lett.* **11**, 385–390 (2011).
- P. Pust, P. J. Schmidt, and W. Schnick, "A revolution in lighting," *Nat. Mater.* **14**, 454–458 (2015).
- I. Akasaki, "Fascinated journeys into blue light," *Int. J. Mod. Phys. B* **29**, 1530014 (2015).
- C.-F. Lu, C.-F. Huang, and C. C. Yang, "Reduced blue shift in screening the quantum-confined stark effect of an InGaN/GaN quantum well with the restrained growth of a light-emitting diode," in *Quantum Electronics and Laser Science Conference* (Optica Publishing Group, USA, 2008), paper JThA64.
- K. Pieniak, M. Chlipala, H. Turski, W. Trzeciakowski, G. Muziol, G. Staszczak, A. Kafar, I. Makarowa, E. Grzanka, S. Grzanka, C. Skierbiszewski, and T. Suski, "Quantum-confined Stark effect and mechanisms of its screening in InGaN/GaN light-emitting diodes with a tunnel junction," *Opt. Express* **29**, 1824–1837 (2021).

15. S. Zhu, S. Lin, J. Li, Z. Yu, H. Cao, C. Yang, J. Li, and L. Zhao, "Influence of quantum confined Stark effect and carrier localization effect on modulation bandwidth for GaN-based LEDs," *Appl. Phys. Lett.* **111**, 171105 (2017).
16. O. Ambacher, J. Majewski, C. Miskys, A. Link, M. Hermann, M. Eickhoff, M. Stutzmann, F. Bernardini, V. Fiorentini, V. Tilak, B. Schaff, and L. F. Eastman, "Pyroelectric properties of Al(In)GaN/GaN hetero-and quantum well structures," *J. Phys. Condens. Matter* **14**, 3399 (2002).
17. D. A. B. Miller, D. S. Chemla, T. C. Damen, A. C. Gossard, W. Wiegmann, T. H. Wood, and C. A. Burrus, "Band-edge electroabsorption in quantum well structures: The quantum-confined Stark effect," *Phys. Rev. Lett.* **53**, 2173–2176 (1984).
18. T. Takeuchi, S. Sota, M. Katsuragawa, M. Komori, H. Takeuchi, H. Amano, and I. Akasaki, "Quantum-confined Stark effect due to piezoelectric fields in GaInN strained quantum wells," *Jpn. J. Appl. Phys.* **36**, L382 (1997).
19. Y. Robin, S. Y. Bae, T. V. Shubina, M. Pristovsek, E. A. Evropitsev, D. A. Kirilenko, V. Yu. Davydov, A. N. Smirnov, A. A. Toropov, V. N. Jmerik, M. Kushimoto, S. Nitta, S. V. Ivanov, and H. Amano, "Insight into the performance of multi-color InGaN/GaN nanorod light emitting diodes," *Sci. Rep.* **8**, 7311 (2018).
20. E. D. Le Boulbar, I. Gîrgel, C. J. Lewins, P. R. Edwards, R. W. Martin, A. Šatka, D. W. E. Allsopp, and P. A. Shields, "Facet recovery and light emission from GaN/InGaN/GaN core-shell structures grown by metal organic vapour phase epitaxy on etched GaN nanorod arrays," *J. Appl. Phys.* **114**, 094302 (2013).
21. S. Li and A. Waag, "GaN based nanorods for solid state lighting," *J. Appl. Phys.* **111**, 071101 (2012).
22. B. O. Jung, S.-Y. Bae, S. Lee, S. Y. Kim, J. Y. Lee, Y. Honda, and H. Amano, "Emission characteristics of InGaN/GaN core-shell nanorods embedded in a 3D light-emitting diode," *Nanoscale Res. Lett.* **11**, 215 (2016).
23. X. Wang, S. Li, M. S. Mohajerani, J. Ledig, H.-H. Wehmann, M. Mandl, M. Strassburg, U. Steegmüller, U. Jahn, J. Lähnemann, H. Riechert, I. Griffiths, D. Cherns, and A. Waag, "Continuous-flow MOVPE of Ga-polar GaN column arrays and core-shell LED structures," *Cryst. Growth Des.* **13**, 3475–3480 (2013).
24. M. Tchernycheva, V. Neplokh, H. Zhang, P. Lavenus, L. Rigutti, F. Bayle, F. H. Julien, A. Babichev, G. Jacopin, L. Largeau, R. Ciechonski, G. Vescovi, and O. Kryliouk, "Core-shell InGaN/GaN nanowire light emitting diodes analyzed by electron beam induced current microscopy and cathodoluminescence mapping," *Nanoscale* **7**, 11692–11701 (2015).
25. A. Vogt, J. Hartmann, H. Zhou, M. S. Mohajerani, S. Fündling, B. Szafranski, H.-H. Wehmann, A. Waag, T. Voss, T. Schimpke, A. Avramescu, and M. Strassburg, "Recombination dynamics in planar and three-dimensional InGaN/GaN light emitting diode structures," *J. Mater. Res.* **32**, 2456–2463 (2017).
26. H.-Y. Ryu, "Effect of internal polarization fields in InGaN/GaN multiple-quantum wells on the efficiency of blue light-emitting diodes," *Jpn. J. Appl. Phys.* **51**, 09MK03 (2012).
27. J.-I. Shim and D.-S. Shin, "Measuring the internal quantum efficiency of light-emitting diodes: Towards accurate and reliable room-temperature characterization," *Nanophotonics* **7**, 1601–1615 (2018).
28. E. A. Evropitsev, D. R. Kazanov, Y. Robin, A. N. Smirnov, I. A. Eliseyev, V. Y. Davydov, A. A. Toropov, S. Nitta, T. V. Shubina, and H. Amano, "State-of-the-art and prospects for intense red radiation from core-shell InGaN/GaN nanorods," *Sci. Rep.* **10**, 19048 (2020).
29. J.-H. Kim, Y.-H. Ko, J.-H. Cho, S.-H. Gong, S.-M. Koa, and Y.-H. Cho, "Toward highly radiative white light emitting nanostructures: A new approach to dislocation-eliminated GaN/InGaN core-shell nanostructures with a negligible polarization field," *Nanoscale* **6**, 14213–14220 (2014).
30. Lumerical Solution Inc., "Micro-LED," (Lumerical Solution Inc.), <https://optics.ansys.com/hc/en-us/articles/360053540493-Micro-LED> (Accessed Date: Mar. 24, 2023).
31. H.-Y. Ryu, "Evaluation of light extraction efficiency of GaN-based nanorod light-emitting diodes by averaging over source positions and polarizations," *Crystals* **8**, 27 (2018).
32. H. Huang, H. Hu, H. Wang, and K. Geng, "Enhanced light output of dipole source in GaN-based nanorod light-emitting diodes by silver localized surface plasmon," *J. Nanomater.* **2014**, 180765 (2014).
33. J. R. Riley, S. Padalkar, Q. Li, P. Lu, D. D. Koleske, J. J. Wiener, G. T. Wang, and L. J. Lauhon, "Three-dimensional mapping of quantum wells in a GaN/InGaN core-shell nanowire light-emitting diode array," *Nano Lett.* **13**, 4317–4325 (2013).
34. S. Adachi, *Optical constants of crystalline and amorphous semiconductors: numerical data and graphical information* (Springer New York, USA, 1999).
35. E. F. Schubert, *Light-emitting Diodes*, 2<sup>nd</sup> ed. (Cambridge, UK, 2006).
36. S. A. Kazazis, E. Papadomanolaki, and E. Iliopoulos, "Polarization-engineered InGaN/GaN solar cells: realistic expectations for single heterojunctions," *IEEE J. Photovoltaics* **8**, 118–124 (2017).
37. J. K. Sprenger, H. Sun, A. S. Cavanagh, A. Roshko, P. T. Blanchard, and S. M. George, "Electron-enhanced atomic layer deposition of thin films at room temperature," *J. Vac. Sci. Technol.* **36**, 01A118 (2013).
38. S. O. Kasap, *Optoelectronics and Photonics*, 2<sup>nd</sup> ed. (Pearson Education, UK, 2013).
39. S.-U. Kim, J.-K. Oh, D.-Y. Um, B. Chandran, C.-R. Lee, and Y.-H. Ra, "Sub-micron monolithic full-color nanorod LEDs on a single substrate," *IEEE Photonics J.* **15**, 2200205 (2023).
40. T. Nobis and M. Grundmann, "Low-order optical whispering-gallery modes in hexagonal nanocavities," *Phys. Rev. A* **72**, 063806 (2005).
41. Z. Wang and B. Nabet, "Nanowire optoelectronics," *Nanophotonics* **4**, 491–502 (2015).